



0883-2927(94)00026-3

## Welded tuff porosity characterization using mercury intrusion, nitrogen and ethylene glycol monoethyl ether sorption and epifluorescence microscopy

MICHAEL M. REDDY

U.S. Geological Survey - WRD, 3215 Marine Street, Boulder, CO 80303, U.S.A.

HANS C. CLAASSEN

U.S. Geological Survey - WRD, P.O. Box 25046, MS 412, Denver-Federal Center, Denver, CO 80225, U.S.A.

and

DAVID W. RUTHERFORD and CARY T. CHIOU

U.S. Geological Survey - WRD, 5293 Ward Road, Arvada, CO 80002, U.S.A.

(Received 17 September 1993; accepted in revised form 5 May 1994)

**Abstract**—Porosity of welded tuff from Snowshoe Mountain, Colorado, was characterized by mercury intrusion porosimetry (MIP), nitrogen sorption porosimetry, ethylene glycol monoethyl ether (EGME) gas phase sorption and epifluorescence optical microscopy. Crushed tuff of two particle-size fractions (1–0.3 mm and less than 0.212 mm), sawed sections of whole rock and crushed tuff that had been reacted with 0.1 N hydrochloric acid were examined. Average MIP pore diameter values were in the range of 0.01–0.02  $\mu\text{m}$ . Intrusion volume was greatest for tuff reacted with 0.1 N hydrochloric acid and least for sawed tuff. Cut rock had the smallest porosity (4.72%) and crushed tuff reacted in hydrochloric acid had the largest porosity (6.56%). Mean pore diameters from nitrogen sorption measurements were 0.0075–0.0187  $\mu\text{m}$ . Nitrogen adsorption pore volumes (from 0.005 to 0.013  $\text{cm}^3/\text{g}$ ) and porosity values (from 1.34 to 3.21%) were less than the corresponding values obtained by MIP. More than half of the total tuff pore volume was associated with pore diameters  $<0.05 \mu\text{m}$ . Vapor sorption of EGME demonstrated that tuff pores contain a clay-like material. Epifluorescence microscopy indicated that connected porosity is heterogeneously distributed within the tuff matrix; mineral grains had little porosity. Tuff porosity may have important consequences for contaminant disposal in this host rock.

### INTRODUCTION

Rock porosity, a geological parameter that influences fluid movement, has important implications for several earth science areas including the use of the subsurface for containment of hazardous waste (NATIONAL ACADEMY OF SCIENCE, 1988; FRIND and SUDICKY, 1981; MACKAY *et al.*, 1985) and for disposal of nuclear waste (YANAGISAWA and SAKAI, 1988; FIGFORD and CHAMBRE, 1991; WINOGRAD, 1990; LIESER, 1991; BUDDEMEIER *et al.*, 1991). In nuclear waste disposal, for example, porosity and pore-size distribution determine the surface area of rock which in turn affects the extent of rock–water interactions. Radioisotope movement in the subsurface is retarded in proportion to its retention by reactive sites on the rock surfaces along the waste-flow path. However, measurement of rock surface area and porosity at present (1994) contributes significant uncertainty to waste disposal planning (CAPE and KIBBY, 1990).

The surface areas of solids are usually determined by gas adsorption methods such as the Brunauer–Emmett–Teller (BET) method using inert gases

(BRUNAUER *et al.*, 1938; WHITE and PETERSON, 1990; DAVIS and KENT, 1990; CHIOU *et al.*, 1990). The BET method defines the intrinsic surface area of a solid that is external to the material and which can be used to interpret the adsorption and reaction kinetics of chemical species on simple minerals such as calcite (REDDY *et al.*, 1981). When minerals contain smectite or expanding clay components, polar vapors or liquids (e.g. water) can penetrate into the interior of the solids, through a cation–solvent (ion–dipole) interaction, in addition to adsorption on the intrinsic (external) surfaces. The extent of this solvation effect is a function of the smectite (or expanding clay) content, which can be estimated from the vapor sorption of a polar liquid such as ethylene glycol (EG) or EGME in excess of the adsorption capacity for an inert gas (such as  $\text{N}_2$ ) (CHIOU *et al.*, 1993). We feel that investigations are needed to relate rock properties, such as pore size and pore size distribution, to factors that affect rock–water interaction such as rock surface area.

Previously, we reported specific surface areas for welded tuff from Snowshoe Mountain, Colorado

(REDDY and CLAASSEN, 1994) and results of dissolution experiments using this tuff over a range of solution compositions (REDDY and WERNER, 1987). In this report we summarize mercury intrusion and nitrogen gas sorption porosimetry results for tuff from the summit of Snowshoe Mountain. Vapor sorption of EGME identified a clay-like material in tuff pores, and epifluorescence microscopy identified porous regions of the tuff matrix.

## MATERIALS AND METHODS

A 10 kg slab of welded tuff from the base of a soil column, 1.9 m below land surface, near the summit of Snowshoe Mountain (elevation about 3400 m), near Creede, Colorado, was used in this study (CLAASSEN *et al.*, 1983). Tuff sample preparation and hydrochloric acid reaction conditions are described elsewhere (REDDY and WERNER, 1987). Hydrochloric acid was selected as a reaction medium which would produce a measurable change in tuff porosity. Two size fractions (1–0.3 mm, termed "coarse", and less than 0.212 mm, termed "fine") of crushed and sieved tuff were selected for porosimetry measurements. Rock was also cut into small slabs (referred to as cut tuff) with a diamond saw for porosity measurements with minimum pretreatment.

### Mercury intrusion porosimetry (MIP)

Pore size and pore size distributions are commonly measured by physical adsorption of a gas (usually  $N_2$  at its boiling point) or mercury intrusion porosimetry (MIP). Materials exhibiting a wide range of pore sizes require both methods for the most reliable results, since the precision of results given by either method decreases near the limits of its respective pore size spectrum (LOWELL and SHIELDS, 1991).

Mercury intrusion porosimetry is based on the behavior of non-wetting liquids in capillaries. Pores are modeled as an array of cylindrical capillaries of differing radii, randomly oriented. For mercury the contact angle,  $\Omega$ , is greater than  $90^\circ$ . In this situation, interfacial tension opposes the entrance of liquid into the pore. This opposition must be overcome by external pressure. At equilibrium a relation between the pore radius ( $r$ ) and the applied pressure ( $P$ ) exists (the Washburn equation):

$$r \times P = 2\gamma \cos \Omega.$$

Contact angle,  $\Omega$ , and surface tension,  $\gamma$ , of mercury were  $130^\circ$  and 474 dyne/cm, respectively, in these experiments.

In MIP, the volume of mercury,  $v$ , taken up by the solid is measured as the applied pressure,  $P$ , is gradually increased. By use of the Washburn equation, a relation between  $v$  and  $r$  can be derived. The value of  $v_i$  at any pressure value is termed the cumulative pore volume. The pore-size distribution in the material is given by plotting  $dV/dr$  (incremental intrusion volume) vs  $r$ . A discussion of the applications of the Washburn equation to the interpretation of mercury porosimetry data has been given by LOWELL and SHIELDS (1991).

A Micromeritics Autopore II manufactured by the Micromeritics Instrument Corporation, 800 Goshen Springs Road, Norcross, Georgia, was used for MIP. (The use of trade names is for identification purposes only and does not constitute endorsement by the U.S. Geological Survey.) Procedures were those described by the manufacturers and followed the methods described in ASTM Method C 699, Parts 106–116 and summarized by LOWELL

and SHIELDS (1991). Porosity and pore size distributions, by MIP, were done by the Coors Brewing Company, Analytical Laboratory, Golden, Colorado. MIP measured pores with diameter in the size range 100–0.0040  $\mu\text{m}$ .

### Nitrogen adsorption

A Model 2200 Automatic Surface Area Analyzer, manufactured by the Micromeritics Instrument Corporation was used for low-temperature nitrogen adsorption measurements. Procedures were those described by the manufacturer and followed the methods described by ASTM Method D3037, Parts 14–18 and summarized by LOWELL and SHIELDS (1991). Determinations were done by the Coors Brewing Company, Analytical Laboratory, Golden, Colorado. Nitrogen adsorption measures pore diameters in the size range 0.1500–0.0020  $\mu\text{m}$ .

Nitrogen surface areas for samples used in the EGME procedure (discussed in the next section) were determined using the Gemini 2360 Surface Area Analyzer manufactured by Micromeritics Instrument Company (CAMP and STANLEY, 1991).

### Ethylene glycol monoethyl ether (EGME) gas phase sorption

The apparatus and procedure used for determination of vapor uptake by soils and minerals has been described previously (CHOU *et al.*, 1988). Briefly, experiments consist of equilibrating the solid with EGME vapor in a sorption chamber containing a Cahn Model 2000 electrical microbalance to which a test solid sample (sorbent) is hung in a small glass cup. The sorbent sample was heated to  $100^\circ\text{C}$  for 6–8 h inside the chamber and then cooled to room temperature for 6–8 h under a vacuum of  $10^{-6}$  torr to remove moisture and to determine the "dry sample weight". Typically, 100–500 mg of sample was used in sorption experiments. EGME, purified by vacuum distillation to remove residual air, was then introduced into the sorption chamber. The change in sample weight resulting from the vapor uptake at equilibrium was recorded as an electrical signal from the balance. The partial pressure of EGME at the point of vapor-sample equilibrium was recorded by a Baratron pressure gauge.

### Epifluorescence microscopy

Pore structures are typically identified using optical microscopy. Thin sections used in this technique are prepared by impregnating rock with a blue-dyed epoxy. However, pores smaller than several micrometers in diameter, or pores within the tuff cannot be seen with this technique. Incident-light fluorescence microscopy, in contrast, distinguishes narrow pores and pores that lie at some distance below the rock surface.

Materials, methods and procedures employed for incident-light fluorescence microscopy were similar to those described elsewhere (RUZYLA and JEZEK, 1987; SOEDER, 1990; GIES, 1987). Staining the impregnation epoxy with a mixture of rhodamine B dye and blue dye and using incident blue light to illuminate the impregnated thin sections causes rhodamine B to fluoresce with a brilliant red-orange color. Impregnated pores at the surface and within the section fluoresce and become an emission source, causing sub-micron impregnated pores to become visible.

Coarse tuff, evacuated at 0.1 atmospheres pressure, was impregnated with epoxy and resin (Dow # 331 Epoxy with *n*-butylglycidyl ether as a thinner and diethylene triamine as a hardener). A mixture of equal parts of blue dye powder and rhodamine powder was added to the epoxy in the same

Table 1. Mercury porosimetry values for average pore diameter, pore volume and porosity for coarse crushed and cut Snowshoe Mountain welded tuff

Sample treatment	Intrusion volume (cm <sup>3</sup> /g)	Average pore diameter ( $\mu$ m)	Bulk density (g/ml)	Skeletal density (g/ml)	Porosity (%)
Unreacted	0.024	0.020	2.40	2.54	5.80
Reacted in 0.1 N HCl	0.027	0.011	2.38	2.55	6.56
Cut unreacted	0.019	0.011	2.47	2.60	4.72

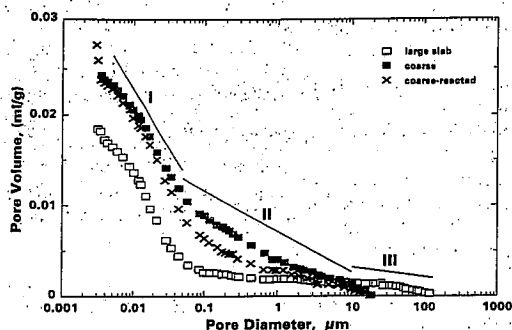


Fig. 1. Mercury intrusion porosimetry cumulative intrusion in ml/g plotted vs pore diameter in  $\mu$ m for Snowshoe Mountain welded tuff:  $\square$  cut rock;  $\blacksquare$  coarse tuff, unreacted; and  $\times$  tuff reacted in 0.1 N hydrochloric acid.

portion as the blue dye alone in conventional sections. The epoxy was cured in a closed chamber pressurized at 1500 psi (100 atmospheres) to minimize unfilled pores. Thin sections cut from blocks of epoxy impregnated rock were examined using a Nikon Labophot-pol Microscope with a Nikon UFX-II 35-mm camera system and Episcope fluorescence attachment with a blue-violet filter cube.

#### X-ray diffraction analysis

X-ray diffraction analysis for mineral species identification was done using an automated Siemens Diffractometer 500 in the step scan mode. Measurement parameters were: start angle 2°, stop angle 20°, step 0.020° and count time 2.0 s.

## RESULTS AND DISCUSSION

### Mercury intrusion porosimetry (MIP)

Snowshoe Mountain welded tuff MIP results are summarized in Table 1. Average MIP pore diameter values were in the range 0.01–0.02  $\mu$ m. Bulk and skeletal densities were approximately 2.4 and 2.6 g/cm<sup>3</sup>, respectively. Crushing and/or dissolution increased available tuff intrusion volume. Measured intrusion volume was greatest for tuff reacted with 0.1 N hydrochloric acid and was least for cut tuff. Porosity exhibited the same trend as intrusion volume—cut rock had the smallest porosity (4.72%) and tuff reacted in hydrochloric acid had the greatest porosity (6.56%) (Table 1).

Cumulative mercury intrusion volumes are plotted vs the log of pore diameter in Fig. 1. The plotted

points approximately exhibit linear segments, designated in terms of pore diameter, as follows: I, 0.01–0.05  $\mu$ m; II, 0.5–10  $\mu$ m; and III, 10–100  $\mu$ m (Fig. 1). Linear segments in these plots differ for each treatment, reflecting pore modification associated with physical and chemical changes within the rock. Linear segments illustrate that tuff pore diameters in these ranges have a logarithmic normal distribution. Linear segment I and Fig. 1 illustrates that most tuff pore volume is due to pores having diameters from about 0.05 to 0.002  $\mu$ m.

Log-normally distributed variables in earth science are characterized by the fact that, compared with the arithmetic mean value, most of the values are small, but a few are very large (KOCH and LINK, 1980; DIEM, 1962). BARRON (1989) demonstrated that rock fracturing, a process which extends over a large range of linear dimensions, is an iterative process in which pre-existing fractures affect the formation of subsequent fractures. We believe that an iterative process involving redistribution of entrained gas, and phase changes in the cooling tuff lead to the log-normal intrusion volume–(log) pore diameter distributions shown in Fig. 1 (REDDY and CLAASSEN, 1994).

Cut rock has large pore diameters (100  $\mu$ m, Fig. 1, segment III); pores of this size are also apparent in photomicrographs of cut tuff (Reddy, USGS, unpublished data, 1992). About 10% of the total MIP intrusion volume is associated with pore diameters in the size range from 10 to 100  $\mu$ m. These large diameter pores will contribute most to water movement through the tuff. Pore diameters in the range 1–10  $\mu$ m contribute little to the intrusion volume (Fig. 1, segment II). The largest contribution to tuff intrusion volume is associated with pores having a diameter of 1  $\mu$ m or less (Fig. 1).

Maximum pore size is considerably smaller in the coarse tuff (20  $\mu$ m) than in the cut rock (100  $\mu$ m). Grinding tuff will tend to eliminate larger pores because the stress imposed by grinding tends to cause fractures along larger pores. This breaks the tuff into smaller fragments in which larger pores no longer exist. In comparison with the cut rock, crushed samples have a greater contribution to pore volume from pores with diameters in the range 0.05–10  $\mu$ m. Since crushed tuff has a larger intrusion volume than cut tuff, crushing appears to allow mercury intrusion into pores that were unavailable in cut tuff.

Linear segments in the pore volume vs log pore

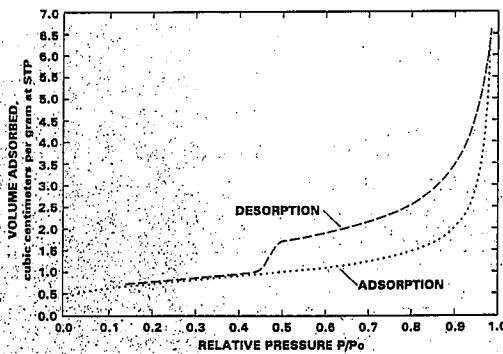


Fig. 2. Nitrogen sorption curves for coarse tuff from Snowshoe Mountain illustrating hysteresis at  $p/p_0 > 0.5$ .

diameter plot (Fig. 1) decrease after reaction with hydrochloric acid; pore volumes associated with pore diameters in the range  $0.1\text{--}1\ \mu\text{m}$  had the largest change.

#### Nitrogen adsorption

Nitrogen gas adsorption and desorption isotherms also depict pore diameter and pore volume distributions in rocks. In particular, the presence of hysteresis in nitrogen adsorption isotherms is due to adsorption in pores with diameters  $< 0.05\ \mu\text{m}$  (Fig. 2) (GREGG and SING, 1982). All tuff examined here exhibited hysteresis, with a characteristic break point in the desorption leg of the curve at  $p/p_0 = 0.45\text{--}0.5$  (Fig. 2). Mean pore diameters calculated from nitrogen sorption measurements were  $0.0075\text{--}0.0187\ \mu\text{m}$  (Table 2). Pore volumes (from  $0.005$  to  $0.013\ \text{cm}^3/\text{g}$ ) and porosity values (from  $1.34$  to  $3.21\%$ ) calculated from nitrogen adsorption were less than values determined by mercury intrusion porosimetry (Tables 1 and 2). Differences between MIP and nitrogen sorption arise because large pores are not measured during nitrogen sorption.

Average pore diameters for the coarse and fine fractions are similar (Table 2). Cut rock average pore diameter is larger than that for the crushed material because, as discussed above, large pores in the rock are eliminated by crushing. Tuff reacted in  $0.1\ \text{N}$  hydrochloric acid had the smallest average pore diameter. As will be discussed, pore volume distribution for tuff reacted with  $0.1\ \text{N}$  hydrochloric acid is broadened for the smallest size pores. This increase

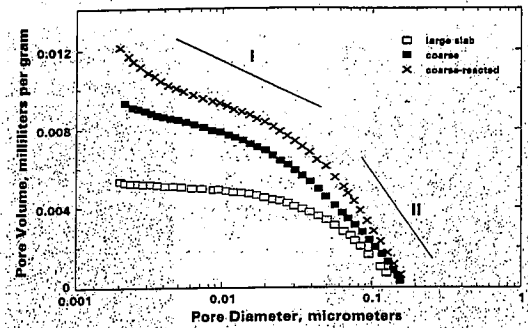


Fig. 3. Nitrogen sorption plots for tuff from Snowshoe Mountain, Colorado. Adsorbed volume in  $\text{ml/g}$  at STP plotted as a function of pore diameter in  $\mu\text{m}$ : cut tuff; coarse tuff; tuff reacted in  $0.01\ \text{N}$  hydrochloric acid. Linear segments correspond to pore diameter ranges as follows: I,  $0.003\text{--}0.05\ \mu\text{m}$ ; and II,  $0.05\text{--}0.2\ \mu\text{m}$ .

in the number of small pores shifts the average pore diameter to a smaller value.

Cut tuff pore volume is about half that of the crushed tuff. Differences between cut and the crushed tuff imply that, in agreement with the MIP data presented earlier, crushing increased submicron pore diameter accessibility to nitrogen gas. However, additional crushing to produce the fine-size fraction increased the pore volume only slightly ( $11\%$ , Table 2). Cumulative nitrogen-adsorption volume vs. (log) pore diameter plots (Fig. 3) have two (log) linear segments similar to data for mercury intrusion volume vs. (log) pore diameter obtained with MIP (Fig. 1). As shown in Fig. 3, for similar pore diameter intervals submicron pore volume increases in the order: cut tuff, coarse tuff and tuff reacted with hydrochloric acid.

Pore volumes plotted vs. (log) pore diameter give peaks that identify pore diameters contributing most to total pore volume (Figs 4A–D). Features distinctive of Snowshoe Mountain tuff pore volume-pore diameter relations illustrated in these plots are:

- (1) a sharp peak in total pore volume in the pore diameter range  $0.0035\text{--}0.005\ \mu\text{m}$ ; and
- (2) a broad, asymmetric peak between  $0.0040$  and  $0.100\ \mu\text{m}$  centered near  $0.05\ \mu\text{m}$ .

Differential pore volume peaks identify the modal (most frequent) pore diameter populations contributing to the total pore volume (Fig. 4). Pore diameters with differential pore volume values near zero have few pores in that size range contributing to pore volume. A broad peak in differential pore volumes,

Table 2. Nitrogen adsorption-desorption, average pore diameter, pore volume and porosity for Snowshoe Mountain welded tuff

Sample treatment	Pore volume ( $\text{cm}^3/\text{g}$ )	Average pore diameter ( $\mu\text{m}$ )	Porosity (%)
Coarse tuff, unreacted	0.0099	0.0118	2.38
Fine tuff, unreacted	0.01158	0.0115	2.77
Coarse tuff, reacted with $0.1\ \text{N}$ HCl	0.01348	0.0075	3.21
Cut tuff, unreacted	0.0054	0.0187	1.34

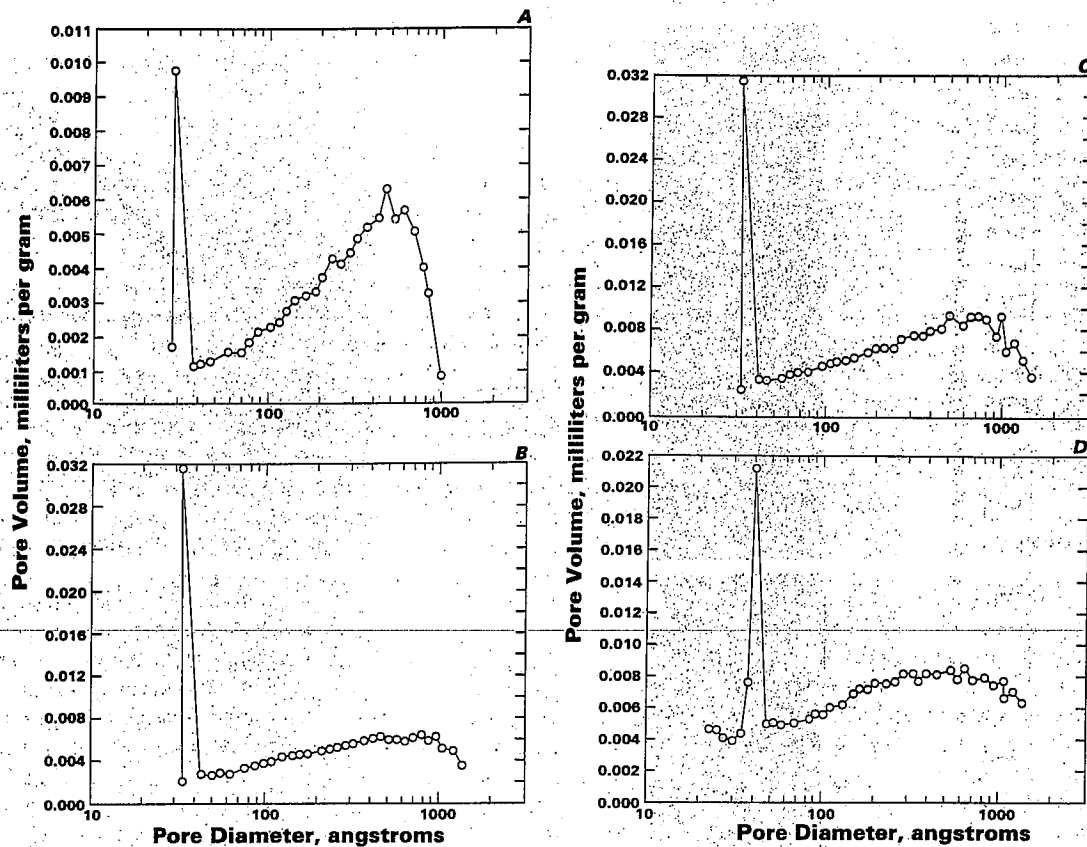


Fig. 4. Nitrogen sorption differential desorption pore volume plotted as a function of pore diameter: (A) cut tuff; (B) coarse tuff, unreacted; (C) fine tuff, unreacted; and (D) tuff, reacted in 0.1 N hydrochloric acid.

over a range of pore diameters, corresponds to a smooth distribution of pore diameters contributing to the cumulative pore volume. Area under a segment of the differential pore volume curve is proportional to pore volumes associated with pore diameters in that segment.

The pore volume peak for pore diameters near  $0.0035 \mu\text{m}$  in Fig. 4 arises because of a submicron matrix quartz-phase change, and corresponding volume decrease, that occurred during tuff cooling (REDDY and CLAASSEN, 1994). The pore volume distribution for larger pore diameters may develop because of trapped gas redistribution during ash welding, a process which may be similar to that described by Anderson for the Bishop tuff (ANDERSON, 1991).

Cut tuff (Fig. 4A) has a smaller volume for the smallest pore diameters ( $0.0035 \mu\text{m}$ ) than coarse tuff (Fig. 4B) suggesting that the smallest pores in the cut tuff are not fully accessible to gas adsorption. On the other hand, the broad pore volume peaks centered at approximately  $0.05 \mu\text{m}$  have similar differential volumes for the cut and the coarse tuff; larger pores appear to be accessible in both samples. Fine tuff (Fig. 4C) has a similar pore volume to that of the coarse fraction (Fig. 4B).

Tuff reacted with hydrochloric acid (Fig. 4D) exhibited a pore volume peak for the smallest diameter pores which differed from other samples examined (Figs 4A-C). This pore volume peak broadened and shifted in maximum value from  $0.0035 \mu\text{m}$  in the cut tuff to  $0.0040 \mu\text{m}$  following reaction with hydro-

Table 3. Specific surface area values for fine ( $<0.212 \text{ mm}$  fraction) Snowshoe Mountain welded tuff before and after reaction with 0.1 N hydrochloric acid. Surface area determinations employed nitrogen and ethylene glycol monoethylether (EGME) gas sorption procedures

Rock treatment	Specific surface area ( $\text{m}^2/\text{g}$ ) nitrogen adsorption	Apparent surface area ( $\text{m}^2/\text{g}$ ) EGME sorption
None	2.2 ( $\pm$ ) 0.2	15.0 ( $\pm$ ) 0.5
0.1 N HCl	11.0 ( $\pm$ ) 0.5	10.0 ( $\pm$ ) 0.5

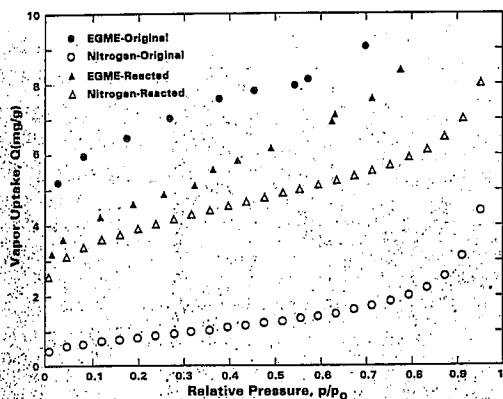


Fig. 5. Nitrogen adsorption and ethylene glycol monoethyl ether (EGME) sorption isotherms for fine tuff unreacted and reacted with 0.1 N hydrochloric acid.

chloric acid. Enlargement of the smallest pore sizes evidently occurred during reaction in 0.1 N hydrochloric acid; this shifted the broad distribution of pore volumes to a larger pore diameter. This change in pore volume following reaction with hydrochloric acid is clear evidence that, under the conditions employed here, the tuff pores with the smallest diameter interact with the surrounding aqueous solution.

#### EGME sorption

MIP and nitrogen adsorption porosimetry data quantify porosity in Snowshoe Mountain welded tuff. However, these techniques give no direct information concerning the spatial distribution and the nature of tuff porosity. For example, Snowshoe Mountain tuff porosity has been attributed to the tuff matrix (REDDY and CLAASSEN, 1994). Gravimetric sorption of EGME and epifluorescence examination of impregnated rock thin sections, give insight into the nature of rock porosity and have been applied to examine the hypothesis that tuff porosity resides in the matrix.

Surface area measurements of clay minerals, based on the retention of EG or EGME, and the uptake of water, have resulted in values that are much greater than measurements by standard BET  $N_2$  method (MCNEAL, 1964; QUIRK, 1955; CHIOU *et al.*, 1993). This observation is evidence that EG and EGME sorption also occurs at the clay ion-exchange site (i.e. the clay interlayer spaces) as well as on the pre-existing clay surface. It is assumed that EGME uptake in excess of that expected from monolayer coverage of a surface is indicative of the presence of clay-like minerals (CHIOU *et al.*, 1993).

Nitrogen and EGME uptake by tuff have similarly-shaped sorption isotherms (Fig. 5). Both have linear BET function plots, except that EGME sorption was greater than nitrogen (on an area basis) and hence

that EGME gave a higher apparent surface area (Table 3). Higher apparent surface areas by the EGME method, in comparison with those by nitrogen adsorption, suggest that an expandable clay is within, or coats, the tuff pores. X-ray diffraction analysis of cut tuff demonstrated an expandable clay (montmorillonite) in the fresh tuff.

Tuff reacted in 0.1 N hydrochloric acid had nearly equivalent nitrogen and EGME sorption and surface-area values [ $11 \text{ m}^2/\text{g}$  (nitrogen) vs  $10 \text{ m}^2/\text{g}$  (EGME) (Table 3)]. Acid reaction presumably removed the clay-like material associated with the tuff pores and hence the acid-treated tuff showed an increase in BET surface area. Because the acid-treated tuff is presumably free of clay material, the apparent surface area of the sample based on a BET plot of the EGME sorption data should be the same as that for a BET plot surface area based on nitrogen adsorption.

#### Epifluorescence microscopy

Photomicrographs (Fig. 6A) of tuff illustrate quartz, biotite, and plagioclase phenocrysts as bright areas; in a mottled texture of the tuff matrix surrounded by blue embedding epoxy. Mineral distribution within tuff grains is heterogeneous. Incident illumination of the same area (Fig. 6B) shows strong red-orange fluorescence in the grain center but little from phenocrysts. The matrix in some grain segments exhibits no fluorescence; elsewhere, matrix fluorescence is intense. Fluorescence, and thus porosity, occurs adjacent to opaque minerals in the matrix (Fig. 6B).

Higher magnification illustrates large and small mineral phenocrysts in the matrix (Fig. 6C). The phenocryst at the right in Figs 6C and D is fractured; however, only segments of these fractures adjacent to the matrix exhibit fluorescence. Connected porosity occurs predominantly in the matrix. Phenocryst fractures show little fluorescence; they have few connected fractures and low porosity. Some segments of tuff matrix have little connected porosity. Matrix porosity is greatest where tuff-flow banding occurs and when matrix is adjacent to opaque minerals. The cause of markedly heterogeneous porosity distribution in the tuff is uncertain, but may be due to tuff deposition, flow and subsequent welding.

#### CONCLUSIONS

A rock from the base of a soil column at the summit of Snowshoe Mountain, near Creede, Colorado (elevation about 3400 m), exhibits high specific surface area due to tuff matrix porosity. More than one-half of the tuff volume as measured by mercury intrusion porosimetry is associated with pore diameters less than  $0.05 \mu\text{m}$ . Tuff matrix appears to

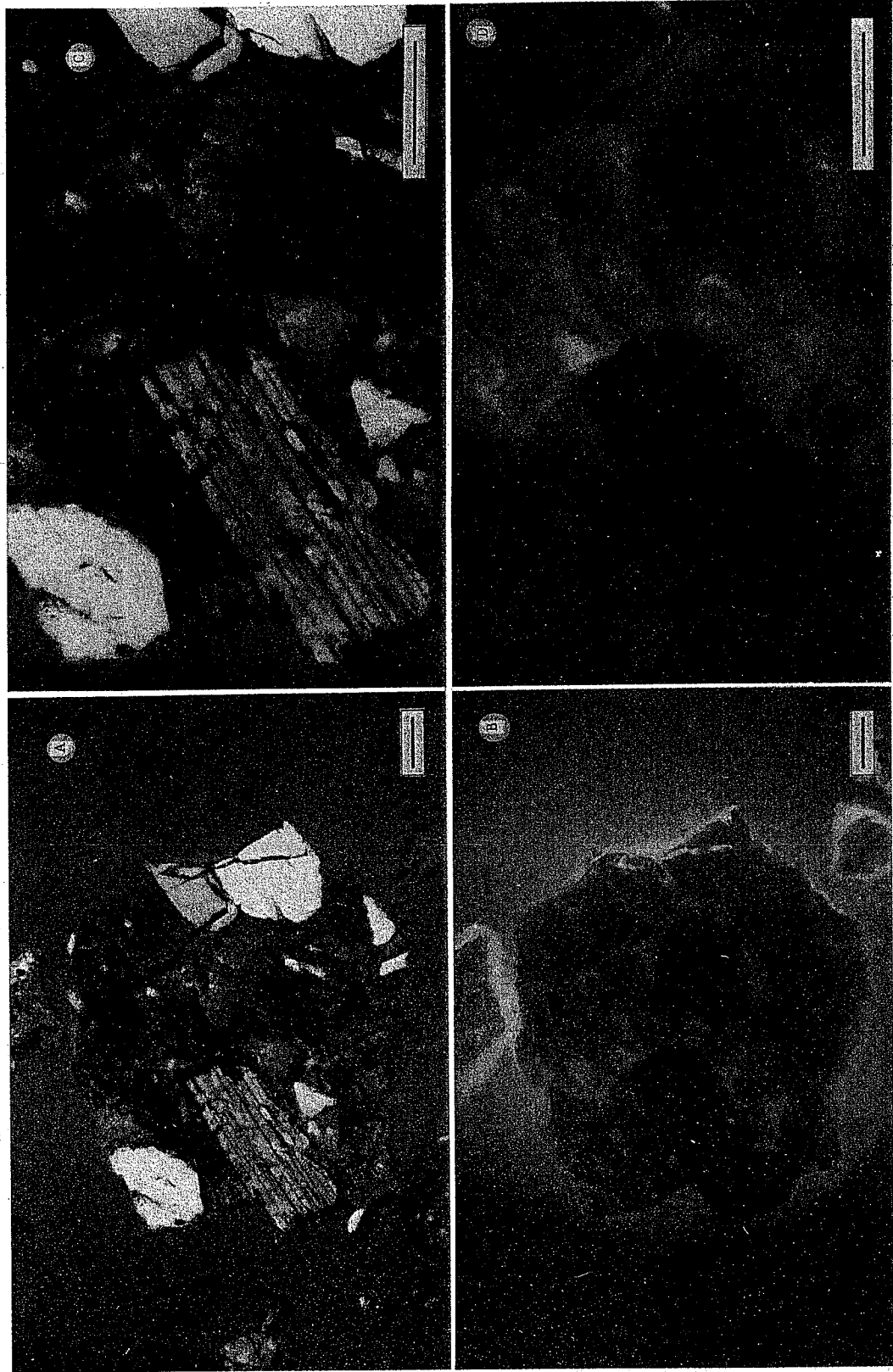


FIG. 6. Photomicrographs of coarse tuff impregnated with blue dyed epoxy containing rhodamine. B. Photographs on the top have transmitted, slightly uncrossed-polarized light illumination and on the bottom epifluorescence illumination. The bar marker is 100  $\mu$ m. Rhodamine dye fluoresces with a red-orange color, showing pores impregnated by the dyed epoxy, in a background of green light when illuminated with blue light.

contain a clay-like material that can be removed by extended dissolution in 0.1 N hydrochloric acid. Epifluorescence microscopy demonstrates that Snowshoe Mountain tuff porosity is heterogeneously distributed within the tuff matrix.

Acid-soluble clay-like materials, present in pores of tuff, can react with aqueous solutions in contact with them. Reactive materials in tuff pores could act to retain waste solutions or alter them in various ways, enhancing containment of chemical or nuclear contaminants. The small size of most tuff pores, their corresponding high surface area and heterogeneous distribution have important implications for transmissivity and contaminant retardation where a welded tuff is the waste disposal host rock.

**Acknowledgements**—The authors acknowledge the assistance of P. Boni, Geology Department, University of Colorado at Boulder, in the preparation of thin sections.

**Editorial handling:** Yousif Kharaka.

## REFERENCES

- ANDERSON A. T., JR (1991) Hourglass inclusions: theory and application to the Bishop Rhyolitic Tuff. *Am. Miner.* **76**, 530–547.
- BARTON C. C. (1989) Fractal characteristics of fracture networks and fluid movement in rock. In *Extended Abstracts Fractal Aspects of Materials — 1989 Proceedings of Symposium — 1989 Fall Meeting of the Minerals Research Society* (eds J. H. KAUFMAN, J. E. MARTIN and P. W. SCHMIDT), p. 71. Materials Research Society, Pittsburgh, Pennsylvania.
- BRÜNAUER S., EMMETT P. H. and TELLER E. (1938) Adsorption of gases in multimolecular layers. *J. Am. chem. Soc.* **60**, 309–319.
- BUDDEMEIER R. W., FINKEL R. C., MARSH K. V., RUGGIERI M. R., REGO J. H. and SILVA R. J. (1991) Hydrology and Radionuclide Migration at the Nevada Test Site. *Radiochim. Acta* **52-53**, 275–282.
- CAMP R. W. and STANLEY H. D. (1991) Advances in measurement of surface area by gas adsorption. *Am. Lab.* **34**, 34–36.
- CAPE J. A. and KIBBY C. L. (1990) On the meaning of surface area measurements for microporous materials. *J. Colloid Interf. Sci.* **138**, 515–520.
- CHIOU C. T., KILE D. E. and MALCOLM R. L. (1988) Sorption of vapors of some organic liquids on soil humic acid and its relation to partitioning of organic compounds in soil organic matter. *Environ. Sci. Technol.* **22**, 298–303.
- CHIOU C. T., LEE J. F. and BOYD S. A. (1990) The surface area of soil organic matter. *Environ. Sci. Technol.* **24**, 1164–1165.
- CHIOU C. T., RUTHERFORD D. W. and MANES, M. (1993) Sorption of N<sub>2</sub> and EGME vapors on some soils, clays, and mineral oxides and determination of sample surface areas by use of sorption data. *Environ. Sci. Technol.* **27**, 1587–1594.
- CLAASSEN H. C., REDDY M. M. and WHITE A. F. (1983) Relationship between precipitation and vadose-zone chemistry in a high-altitude watershed in Colorado. In *Proceedings of the Fifth Annual Participants' Information Meeting, DOE Low-Level Waste Management Program, 30 August–1 September, 1983*, pp. 726–736. U.S. Department of Energy, Contract No. AC07-76ido1570, Idaho Falls, Idaho.
- DAVIS J. A. and KENT D. B. (1990) Surface complexation modeling in aqueous geochemistry. In *Mineral-Water Interface Geochemistry, Reviews in Mineralogy* (eds M. F. HOCCHELLA, JR and A. F. WHITE), Vol. 23, pp. 177–260. Mineralogical Society of America.
- DIEM K. (1962) *Documenta Geigy Scientific Tables*, pp. 164–165. Geigy Pharmaceuticals, Ardsley, New York.
- DYAL R. S. and HENDRICKS S. B. (1950) Total surface of clays in polar liquids as a characteristic index. *Soil Sci.* **69**, 421–432.
- FRIND E. O. and SUDICKY E. A. (1981) Contaminant transport in fractured porous media: analytical solution for a single fracture. *Water Resource Res.* **17**, 555–564.
- GIES R. M. (1987) An improved method for viewing micro-pore systems in rocks with the polarizing microscope. *SPE Form. Eval.* 209–214.
- GREGG S. J. and SING K. S. (1982) *Adsorption, Surface Area and Porosity*. Academic Press, New York.
- KOCH G. S. JR and LINK R. F. (1980) Distributions and transformations. In *Statistical Analysis of Geological Data*, p. 215. Dover Publications, New York.
- LIESER K. H. (1991) Chemistry and Migration Behavior of Actinides and Fission Products in the Geosphere 1. Preface. *Radiochim. Acta* **52**, 1.
- LÖWELL, S. and SHIELDS, J. E. (1991) *Powder Surface Area and Porosity* (3rd edn), Chapman and Hall, New York.
- MACKAY D. M., ROBERTS P. V. and CHERRY J. A. (1985) Transport of organic contaminants in groundwater. *Environ. Sci. Technol.* **19**, 392–394.
- MCNEAL B. L. (1964) Effect of exchangeable cations on glycol retention. *Soil Sci.* **97**, 96–102.
- NATIONAL ACADEMY OF SCIENCE (1988) *Hazardous Waste Site Management: Water Quality Issues*. National Academy Press, Washington, DC.
- PIGFORD T. H., and CHAMBRE P. L. (1991) Near-field mass transfer in geologic disposal systems: A review. In *Scientific Basis for Nuclear Waste Management XI* (eds M. J. APTED and R. E. WESTERMAN), p. 1. Materials Research Society, Pittsburgh, Pennsylvania.
- QUIRK J. P. (1955) Significance of surface areas calculated from water vapor sorption isotherms. *Soil Sci.*, **80**, 423–430.
- REDDY M. M. and CLAASSEN H. C. (1994) Specific surface area of a crushed welded tuff before and after aqueous dissolution. *Appl. Geochem.* **9**, 223–233.
- REDDY M. M., PLUMMER L. N. and BUSENBERG E. (1981) Crystal growth of calcite from calcium bicarbonate solutions at constant carbon dioxide partial pressures and 25 degrees: A test of a calcite dissolution model. *Geochim. cosmochim. Acta* **45**, 1281–1289.
- REDDY M. M. and WERNER M. G. (1987) Data from laboratory dissolution experiments using a welded tuff from Snowshoe Mountain near Creede, Colorado. U.S. Geol. Surv. Open File Rep. 87-550.
- RUZYLKA K. and JEZEK D. I. (1987) Staining method for recognition of pore space in thin and polished sections. *J. sedim. Petrol.* **57**, 777–778.
- SOEDER D. J. (1990) Applications of fluorescence microscopy to study of pores in tight rocks. *Bull. Am. Ass. Petrol. Geol.* **74**, 30–49.
- WHITE A. F. and PETERSON M. L. (1990) The role of reactive surface area characterization in geochemical kinetic models. In *Chemical Modeling of Aqueous Systems II* (eds D. C. MELCHIOR and R. L. BASSETT). *Am. chem. Soc. Symp. Ser.* **416**, 461–475.
- WINOGRAD I. (1990) The Yucca Mountain project: another perspective. *Environ. Sci. Technol.* **24**, 1291–1293.
- YANAGISAWA F. and SAKAI H. (1988) Leaching behavior of a simulated nuclear waste glass in groundwater at 50–240°C. *Appl. Geochem.* **3**, 153–163.